Measurement Science and Technology

100 year anniversary
Measurement Science and Technology

Tilted short-period fibre-Bragg-grating-induced coupling to cladding modes for accurate refractometry

To cite this article: G Laffont and P Ferdinand 2001 *Meas. Sci. Technol.* **12** 765

Meas. Sci. Technol. **12** (2001) 765–770 www.iop.org/Journals/mt PII: S0957-0233(01)20371-3

Tilted short-period fibre-Bragg-grating-induced coupling to cladding modes for accurate refractometry

G Laffont and P Ferdinand

CEA–LIST–DIMRI/SIAR, Centre d'Etudes de Saclay, F 91191 Gif-sur-Yvette, France

E-mail: guillaume.laffont@cea.fr

Received 3 January 2001, accepted for publication 1 March 2001

Abstract
We investigate the changes in the transmission spectrum of long period fibre gratings and tilted short-period fibre Bragg gratings *versus* the refractive index of the surrounding medium. The metrological characteristics of tilted short-period fibre Bragg gratings and an analytical method enabling their potential use in accurate refractometry are discussed.

Keywords: optical fibre sensors, fibre Bragg gratings, refractometry

1. Introduction

Within the past 10 years, fibre Bragg gratings (or FBGs) have shown an increasing potential in guided-wave sensing. They are more and more used as optical transducers spectrally encoding the measurand of interest and the sensor address in optical fibre sensor networks. Due to their intrinsic characteristics, they have opened wide fields of applications such as structure routing in civil engineering and composite materials and are now well known to provide direct strain, temperature or hydrostatic pressure measurements.

Several schemes for refractive index sensing based on FBGs have already been proposed: they rely on etched fibres or side-polished fibres [1, 2]. They exploit the influence of the refractive index of the surrounding medium (within the evanescent field domain) on the effective index of the core mode, and consequently on the Bragg grating's wavelength. However, in order to probe the external medium, the cladding around the grating has to be removed; unfortunately, this process could significantly weaken the optical fibre.

Transmission spectra of FBGs often exhibit discrete dips at wavelengths below the Bragg wavelength. These losses are due to coupling to cladding modes. Whereas such couplings are undesirable in optical communications purposes, they can be enhanced with appropriate in-fibre gratings and turned in good account in refractive index sensing. Up to now, only long-period fibre gratings (LPFGs) have been used for that purpose [3–6]. While similar experiments are reported in the fourth part of this paper, we focus in the fifth part on the response of tilted short-period fibre Bragg gratings (TFBGs) to external refractive index. An analytical method enabling their potential use as chemical and/or biochemical sensors is presented and their metrological characteristics (resolution, repeatability, dynamic and temperature cross-sensitivity) are investigated.

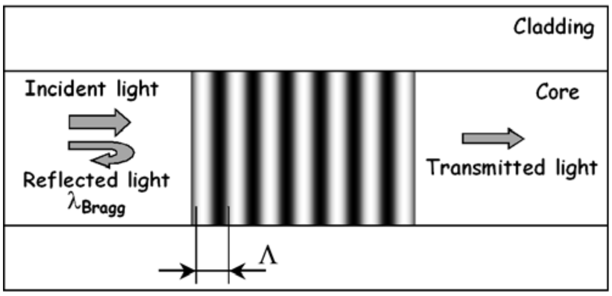

Figure 1. Schematic diagram of a standard fibre Bragg grating reflecting light at the resonance wavelength λ_{Bragg}.

2. Cladding mode coupling with LPFGs and TFBGs

In this part, we will give some explanations on the fundamental properties of LPFGs and TFBGs in comparison to standard FBGs. Indeed both the operating principle and the spectral characteristics of these gratings are quite different.

Standard FBGs consist in a refractive index modulation of the core which periodicity is on the order of $\Lambda = 0.5$ μm: such a device is depicted in figure 1.

As shown in figure 2, typical transmission spectra exhibit resonances at different wavelengths. The main dip corresponds to the so-called Bragg resonance (coupling between the co- and contra-propagating core modes). The other resonances, on the short-wavelength side, are due to coupling between

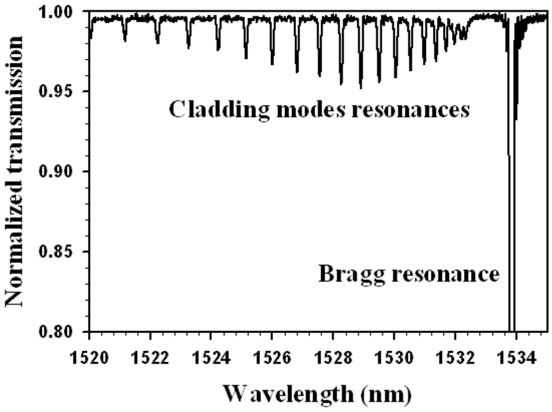

Figure 2. Experimentally measured transmission spectrum of a 8 mm long standard FBG photo-written in a single-mode step-index optical fibre.

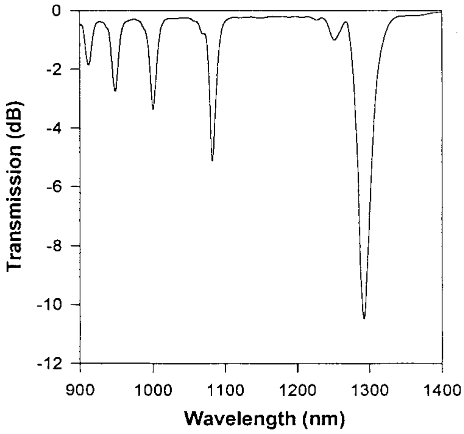

Figure 3. Experimentally measured transmission spectrum of an LPFG with a period of 198 μm (from Bhatia [9]).

the core mode and contra-propagating cladding modes of the fibre. These cladding modes attenuate rapidly along the propagation axis due to the absorption coefficient of the cladding. Therefore these peaks are observable in transmission, but not in reflection.

In contrast, LPFGs are gratings with larger periodicities ranging beyond 100 μm. Due to the small amplitude of the grating vector ($\frac{2\pi}{\Lambda}$) associated with this component, they couple the light from the co-propagating core mode to co-propagating cladding modes: they work in transmission whereas FBGs are reflective components. Figure 3 shows the typical transmission spectrum of such a grating.

TFBGs belong to the short-period grating family ($\Lambda \sim 0.5$ μm) but their index modulation pattern is blazed by an angle θ with respect to the fibre axis [7]. This asymmetry enables and enhances the coupling to circularly and non-circularly symmetric contra-propagating cladding modes. It reduces in return the energy coupling to the contra-propagating core mode (i.e. the Bragg peak). Figure 4 gives the transmission spectrum of a 8 mm long $\theta_{ext} = 16°$-tilted TFBG photo-written in a standard step-index single-mode optical fibre.

All these kinds of grating are classically governed by a phase matching condition which gives the location of the resonance band resulting from the coupling induced between two modes of an optical fibre. This condition involves both the propagation constants of the modes and the amplitude of the grating vector along the propagation axis. Here we consider only the coupling between the core mode and a cladding mode of the fibre. The phase-matching condition can be written either in term of the propagation constants, or in term of the coupling wavelength. For an LPFG, it is expressed as follows:

$$\beta_{core} - \beta_{cladding} = \frac{2\pi}{\Lambda}$$

$$\lambda_{coupling} = (n_{eff,\ core} - n_{eff,\ cladding})\Lambda. \tag{1}$$

For a TFBG, this relation simply becomes

$$\beta_{core} + \beta_{cladding} = \frac{2\pi}{\Lambda} \times \cos\theta$$

$$\lambda_{coupling} = (n_{eff,\ core} + n_{eff,\ cladding})\frac{\Lambda}{\cos\theta}. \tag{2}$$

The $-$ and $+$ signs between the effective indices mean that we consider co- and contra-propagating cladding modes respectively. On the other hand, the amplitude of any resonance is governed by the overlap coefficient between the fields of the two modes.

3. Experiment

The TFBGs used in this experiment were home-made, photo-written in a standard single-mode step-index fibre (previously 150 bar H_2 loaded, for two weeks at room temperature) using an improved Lloyd mirror interferometer [8]. The fibre was fixed on a rotatory stage to carefully adjust the tilt angle, as depicted in figure 5. The angle between the fibre axis and the normal to the fringe pattern, the external tilt angle, is denoted θ_{ext}. It is different from the tilt angle θ of the grating because of the refraction experienced by the UV beam, mainly at the air–cladding interface. The inscription was monitored in real time with a tunable laser diode source. The gratings were then annealed at 80 °C for 24 hours to remove the residual hydrogen.

For LPFGs, our experimental study has been conducted on commercially available UV-written LPFGs.

To determine the cladding mode coupling phenomenon *versus* different refractive indices, we have used Cargille's oils, of which the indices are perfectly known with an accuracy better than 2×10^{-4} r.i.u. (refractive index unit). Three sets of such liquids were available, covering the ranges 1.300–1.398, 1.400–1.458 and 1.460–1.640 in steps of respectively 2×10^{-3}, 2×10^{-3} and 4×10^{-3} r.i.u. For each liquid the refractive index was known at 589 nm (and 25 °C) and deduced for the 1.5 μm window using a Cauchy equation [10] of the form

$$n(\lambda) = A + \frac{B}{\lambda^2} + \frac{C}{\lambda^4}. \tag{3}$$

Each grating was stretched above a microscope slide on which the same amount of liquid was deposited. The whole was thermostated at 25.0 ± 0.1 °C with a Peltier element. The transmission spectra were acquired with a tunable external cavity laser diode.

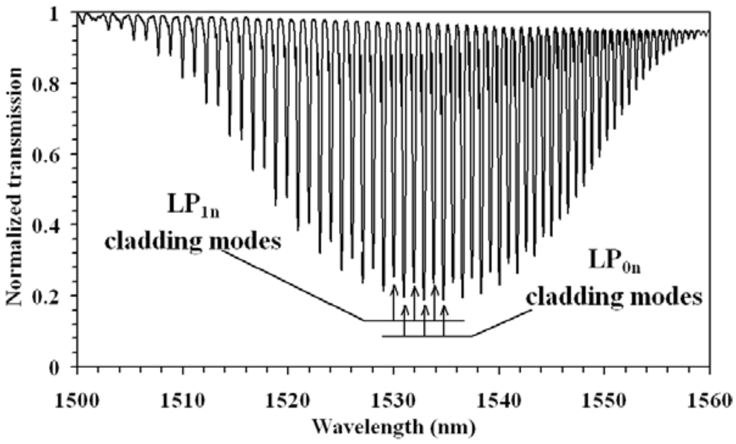

Figure 4. Experimentally measured transmission spectrum of a 8 mm long $\theta_{ext} = 16°$-tilted TFBG surrounded by air.

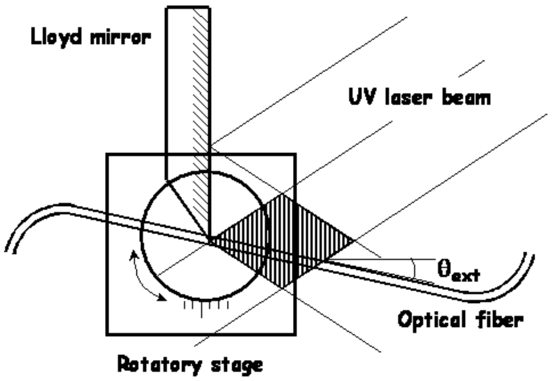

Figure 5. Lloyd mirror interferometer set-up for the photo-writing of TFBGs.

4. Sensitivity of LPFGs to the external refractive index

In this part, we investigate how any change in the refractive index of the medium surrounding the optical cladding affects the spectral properties of LPFGs. The tested grating presented a resonance band at 1532 nm. It was 36 mm in length and has a period of 262 μm.

Figure 6 shows the results obtained for this grating. We can distinguish two domains. First, as the external refractive index n_{ext} changes from 1.0 (air) up to values just below the effective index n_{eff} of the cladding mode, the resonance band experiences a blue shift and its attenuation drops simultaneously. The wavelength shift results from the dependence of n_{eff} on n_{ext}. Therefore, the change of n_{ext} modifies the phase matching condition (1) and hence the coupling wavelength. On the other hand, the decrease of the resonance band's strength is directly related to the decrease of the overlap integral between core and cladding modes, for increasing values of n_{ext}. When n_{ext} is strictly equal to n_{eff}, the resonance vanishes as the coupling occurs with a continuum of radiation modes.

For values of n_{ext} beyond the refractive index of the optical cladding, we observe another resonance at a wavelength slightly higher than the previous resonance's wavelength in air. This band is linked to Fresnel reflections at the interface between the optical cladding and the external medium [6]. Increasing values of n_{ext} do not change the coupling wavelength but increase the attenuation.

The use of LPFGs in refractive index measurements faces several difficulties. The first one is the intrinsic temperature sensitivity (up to ~150 pm °C^{-1}). One way to overcome this temperature cross-sensitivity is to use a standard FBG as a temperature reference grating. Other difficulties arise from strain and bending sensitivities and from the grating's length (typically more than 1–2 cm), preventing punctual measurements. In the following part, we will see that TFBGs are alternative components for refractometry, with satisfactory metrological characteristics and low thermal sensitivity.

5. Refractive index measurement with TFBGs

Following the method briefly depicted in the third part of this paper, five home-made photowritten tilted gratings were tested with external tilt angles ranging from $\theta_{ext} = 8°$ to $16°$. They were about 8 mm long, with a maximum cladding mode attenuation of 80% and a design Bragg wavelength of 1530 nm.

Let us describe the results obtained with the 16°-tilted TFBG. As the external refractive index was changed from $n_{ext} = 1.0$ to 1.3, the centre wavelength λ_i of the dips experienced a red shift ($\Delta\lambda_i \sim 200$ pm) without any significant change of their attenuation. From $n_{ext} = 1.3$ to 1.43, they drop progressively in addition to their spectral shift, to fit a smooth loss curve. Figures 7 and 8 show the transmission spectra obtained for two intermediate values of n_{ext}, i.e. respectively 1.354 and 1.383.

This can be readily explained by the fact that one can assign to any resonance λ_i a discrete cladding mode with an effective index denoted $n_{eff,i}$ which decreases while λ_i decreases. So, when the external refractive index rises and reaches the value $n_{eff,i}$ this mode becomes weakly guided (due to the decrease of the overlap integral between the fundamental guided mode and the $n_{eff,i}$ cladding mode), thereby reducing the amplitude of the coupling coefficient and hence the amplitude of this dip. When n_{ext} is equal to $n_{eff,i}$ then the cladding mode is no longer guided and the coupling now occurs with a continuum of radiation modes.

To take advantage of this phenomenon we have developed an algorithm which determines the lower and upper envelope

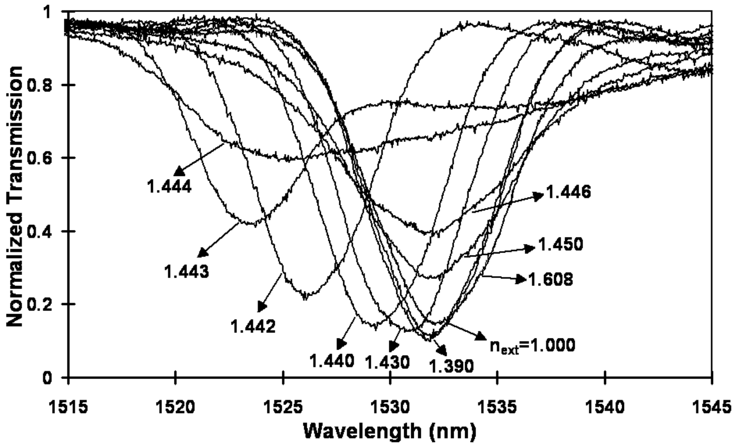

Figure 6. Evolution of the transmission spectrum of a 36 mm long LPFG *versus* the external refractive index.

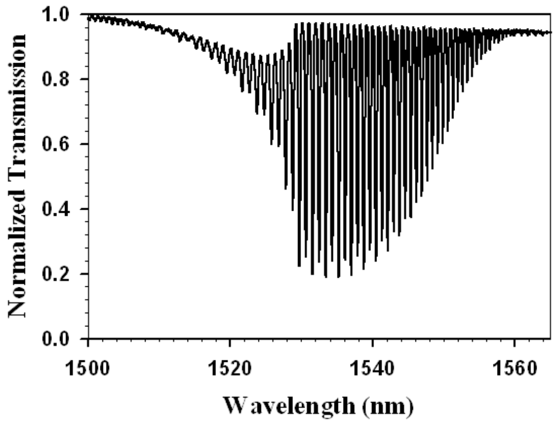

Figure 7. Measured transmission spectrum of a 8 mm long $\theta_{ext} = 16°$-tilted TFBG for an external refractive index value of 1.354.

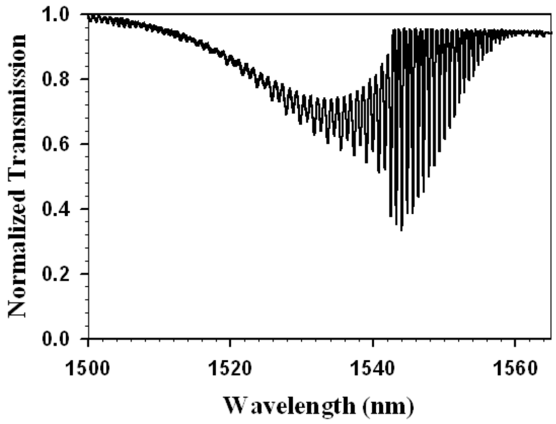

Figure 8. Measured transmission spectrum of a 8 mm long $\theta_{ext} = 16°$-tilted TFBG for an external refractive index value of 1.383.

curves ($\mathcal{E}_{low}$ and $\mathcal{E}_{up}$) and then the normalized area $\mathcal{A}$ of the field delimited by $\mathcal{E}_{low}$ and $\mathcal{E}_{up}$. Instead of monitoring only the wavelength-encoded refractive index shift or the absolute amplitudes, we have chosen to monitor the evolution of this numerical parameter $\mathcal{A}$ defined as follows:

$$\mathcal{A} = \frac{\int_{\lambda_{\min}}^{\lambda_{\max}} [\mathcal{E}_{up}(\lambda) - \mathcal{E}_{low}(\lambda)]\,\mathrm{d}\lambda}{\int_{\lambda_{\min}}^{\lambda_{\max}} [\mathcal{E}_{up}^{n_{ref}}(\lambda) - \mathcal{E}_{low}^{n_{ref}}(\lambda)]\,\mathrm{d}\lambda} \quad (4)$$

where $\lambda_{\min}$ and $\lambda_{\max}$ are the limits of the spectral window of interest (here respectively 1495 nm and 1575 nm), and $\mathcal{E}_{up}^{n_{ref}}$ and $\mathcal{E}_{low}^{n_{ref}}$ are the upper and lower envelope curves obtained for $n_{ref} = n_{ext} = 1.296$ (curve (i) in figure 9).

As the external refractive index increases, the smoothing of the spectrum is equivalent to bringing together the upper and lower envelope curves (figure 9) and so with the decrease of $\mathcal{A}$.

Figure 10 shows the results obtained for the five TFBGs. We can notice that the dynamic can be tailored by properly choosing the tilt angle: Δn_{ext} ranging from 1.32 to 1.42 is achieved with the angle $\theta_{ext} = 16°$. Figure 10 shows also a usual trade-off between range and sensitivity of the refractive index measurement. Furthermore the evolution of $\mathcal{A}$ with n_{ext} can be easily fitted using for example a least squares algorithm, which provides us with the transfer function $\mathcal{A}(n_{ext})$. Since such a calibration curve has been established for any given TFBG, such a grating can be used for sensing purposes.

Experiments have also been performed to estimate some metrological parameters such as repeatability and resolution. For instance, for the $\theta_{ext} = 16°$-tilted SFBG, we have slightly changed the temperature of an $n = 1.390$ Cargille liquid by steps of 0.1 °C which was close to the resolution of our thermostabilization device (Peltier element + feedback loop + thermal insulator) and to the resolution of our temperature sensor. A change of 0.1 °C is equivalent to a change of the refractive index value of roughly 4×10^{-5} (the temperature sensitivity of the liquid is $\frac{\mathrm{d}n}{\mathrm{d}T} = -4.12 \times 10^{-4}$ r.i.u. °C^{-1}). Considering the repeatability, we have put the grating in an $n = 1.373$ liquid at 25 °C and 1000 acquisitions of the transmission spectrum have been performed. 95% of all events were determined within a refractive index range of about 10^{-4}. All these results mean that both the resolution and the repeatability are better than 10^{-4} r.i.u.

The last point we have investigated is the temperature cross-sensitivity of this refractive index sensor. Any change of the temperature of the measured fluid will have two effects. Of course, the first one is the change of the external refractive index, due to the liquid's thermo-optic coefficient, whereas the second one deals with the TFBG's refractometer itself: the spectrum of any TFBG shifts in wavelength with temperature

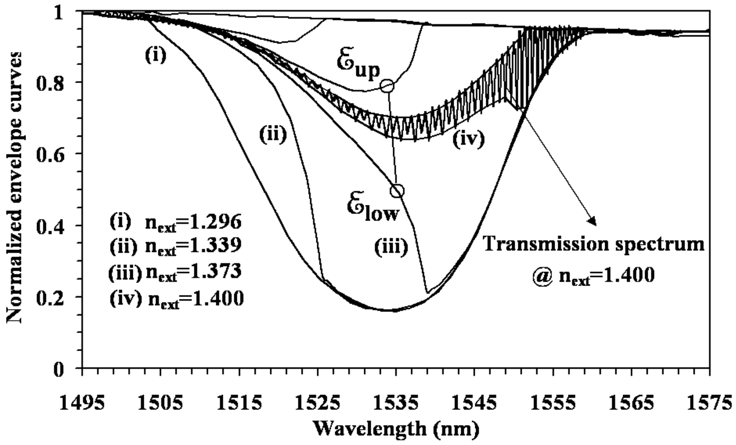

Figure 9. Measured envelope curves of the transmission spectra of a $\theta_{ext} = 16°$-tilted TFBG surrounded by different media.

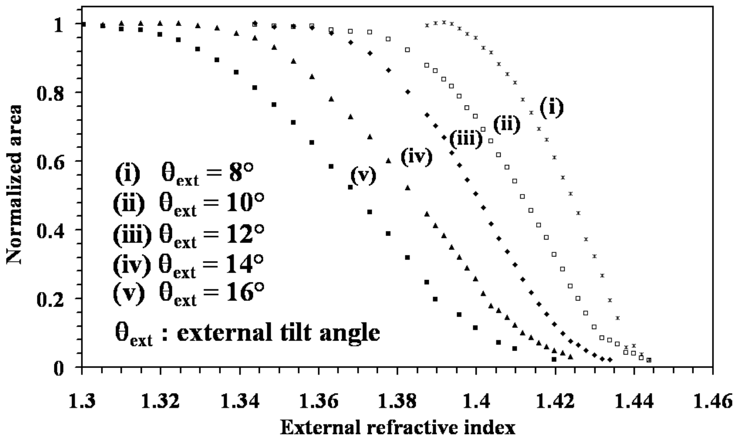

Figure 10. Evolution of $\mathcal{A}$ with the external refractive index for five 8 mm long TFBGs.

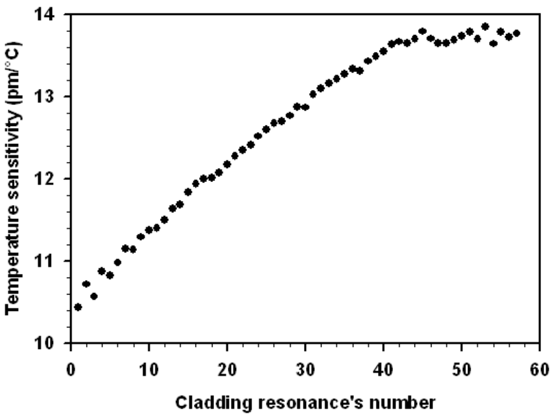

Figure 11. Temperature sensitivity of the cladding resonances of a $\theta_{ext} = 16°$-tilted TFBG surrounded by air.

but without any significant change of the attenuation (in the range 0 °C to 100 °C). Therefore if we assume that the temperature sensitivity (given in pm °C^{-1}) remains the same for each cladding mode resonance, the spectrum's shape will remain unchanged under any thermal fluctuations. Hence, in the same way, the envelope curves and the normalized area $\mathcal{A}$ will not be affected by the TFBG's thermal sensitivity. In reality any cladding mode resonance has a distinct temperature sensitivity. Figure 11 shows the temperature sensitivity of all the cladding resonances present in the spectrum of the $\theta_{ext} = 16°$-tilted TFBG already described in figure 7. The cladding resonances were numbered with respect to their coupling wavelength λ_i: the number $i = 1$ represents the smallest value of λ_i.

Due to these discrepancies, any change in temperature will affect the shape of the spectrum. Therefore $\mathcal{A}$ will change not only because of the thermo-optic induced change in n_{ext} but also because of the TFBG temperature sensitivity itself. In order to evaluate this cross-sensitivity we have computed the value of $\mathcal{A}$ for the $\theta_{ext} = 16°$-tilted TFBG spectrum immersed in an $n = 1.380$ (at 589 nm) Cargille oil thermostated at 25 °C and for the same spectrum with each resonance peak numerically shifted in agreement with their own thermal sensitivity. We obtain a cross-sensitivity of roughly -1.3×10^{-5} r.i.u. °C^{-1}. Experimentally, we have checked this value by measuring the transmission spectra of this grating immersed in the $n = 1.380$ Cargille oil, first at 30 °C and second at 50 °C. Taking into account the thermo-optic coefficient of this oil (-3.44×10^{-4} r.i.u. °C^{-1}), the final thermal error of the measurement is found to be 2×10^{-4} r.i.u. instead of 2.6×10^{-4} r.i.u. This discrepancy can be mostly attributed to the uncertainty on the temperature of the oil (±0.1 °C) and on the thermo-optic coefficient value of the oil, which is only accurately known between 15 °C and 35 °C.

To allow comparison, the same study is performed with the LPFG already mentioned in section 4. Its temperature sensitivity is measured to be 36 pm $^\circ$C^{-1}. As the wavelength sensitivity of LPFGs is highly nonlinear with the external refractive index, we take an intermediate value of -3×10^{-6} r.i.u. pm^{-1} for n_{ext} around 1.438 (at 1550 nm). Hence the cross-sensitivity of this LPFG is -1.1×10^{-4} r.i.u. $^\circ$C^{-1} with respect to -1.3×10^{-5} r.i.u. $^\circ$C^{-1} for the TFBG refractometer. Experimentally we obtain for the LPFG a thermal error of about 10^{-3} r.i.u. instead of 2.2×10^{-3} r.i.u. This value is lower than expected because the wavelength sensitivity decreases with decreasing values of n_{ext}, while the refractive index of the oil decreases with increase of temperature.

Hence the two main advantages of TFBGs in comparison with LPFGs are first their low temperature cross-sensitivity (roughly -1.3×10^{-5} r.i.u. $^\circ$C^{-1} for the grating used) and second the reduced grating length (less than 1 cm).

6. Conclusion

We have investigated the spectral response of an LPFG and of several SFBGs to external refractive index below and beyond the glass cladding index value. A dedicated algorithm has been developed to exploit the sensitivity of SFBGs for the future realization of refractometric chemical and biochemical sensors. Their dynamics depend mainly on the tilt angle and match typically the range 1.32–1.42 for a 16°-tilted grating. Depending on applications, larger Δn_{ext} ranges can be expected with higher angles. We have also shown that the achievable resolution of such transducers is better than 10^{-4} r.i.u. and that the repeatability of the measurements is on the order of 10^{-4} r.i.u. Moreover the thermal cross-sensitivity is roughly -1.3×10^{-5} r.i.u. $^\circ$C^{-1}.

Acknowledgments

The authors would like to thank Professor P Niay from Lille University (France) for helpful discussions and Dr C Martinez for assistance with the FBG photowriting.

References

[1] Asseh A, Sandgren S, Ahlfeldt H, Sahlgren B, Stubbe R and Edwall G 1996 Evanescent field refractive index sensor utilizing a narrow fibre Bragg grating and a tunable DBR laser *Proc. SPIE* **2836** 57–68

[2] Usbeck K, Ecke W, Hagemann V, Mueller R and Willsch R 1999 Temperature referenced fibre Bragg grating refractometer sensor for on-line quality control of petrol products *Proc. 13th Int. Conf. on Optical Fiber Sensors* pp 163–6

[3] Bhatia V and Vengsarkar A M 1996 Optical fiber long-period grating sensors *Opt. Lett.* **21** 692–4

[4] Patrick H J, Kersey A D and Bucholtz F 1998 Analysis of the response of long period fiber gratings to external index of refraction *J. Lightwave Technol.* **16** 1606–12

[5] Pilevar S, DeLisa M P, Zhang Z, Davis C C, Bentley W E and Sirkis J S 2000 Evanescent wave antibody–antigen biosensor based long period fiber Bragg grating *Proc. SPIE* **4185** 314–17

[6] Duhem O, Henninot J F, Warenghem M and Douay M 1998 Demonstration of long-period-grating efficient couplings with an external medium of a refractive index higher than that of silica *Appl. Opt.* **37** 7223–8

[7] Erdogan T and Sipe J E 1996 Tilted fiber phase gratings *J. Opt. Soc. Am.* A **13** 296–313

[8] Martinez C and Ferdinand P 1998 Phase-shifted fibre Bragg grating photowriting using UV phase plate in modified Lloyd mirror configuration *Electron. Lett.* **34** 1687–8

[9] Bhatia V 1996 *PhD Dissertation* Virginia Polytechnic Institute

[10] Bass M, Van Stryland E W, Williams D R and Wolfe W L 1995 *Handbook of Optics* 2nd edn, vol 2 (New York: McGraw-Hill) ch 33, p 26